Letter

Spin-split Andreev bound states and diode effect in an Ising superconductor Josephson junction

Sourabh Patil [1], Gaomin Tang [2,*] and Wolfgang Belzig [1,†]
[1]*Fachbereich Physik, Universität Konstanz, D-78457 Konstanz, Germany*
[2]*Graduate School of China Academy of Engineering Physics, Beijing 100193, China*

(Received 6 November 2024; revised 22 January 2025; accepted 27 January 2025; published 12 February 2025)

The transition-metal dichalcogenides featuring Ising spin-orbit coupling in so-called Ising superconductors offer a unique system to study the interplay of singlet and triplet superconductivity. The presence of high critical fields, spectral properties such as the mirage gap, and field-tunable charge and spin currents in Ising superconductor Josephson junctions are some of the important features. In this Letter, we study an Ising superconductor Josephson junction with a transparent interface and show that Andreev bound states are spin split due to a relative misorientation of in-plane fields in the superconducting contacts. Correspondingly, supercurrent-phase relations display a strongly nonsinusoidal behavior. Introducing additional spin-polarized channels with low transmission results in a nonreciprocal current-phase relation with a diode effect that can be tuned by the in-plane exchange fields. The diode efficiency reaches high values of the order of 40% and is not sensitive to disorder in the junction. Such structures can be realized in van der Waals heterostructures of two-dimensional superconductors and magnets.

DOI: 10.1103/PhysRevB.111.L060502

Introduction. The interplay of superconductivity and magnetism has recently given rise to exciting physics, contributing to the field of superconducting spintronics. Transition-metal dichalcogenides which consist of monolayer to few-layer superconductors with an intrinsic Ising spin-orbit coupling (ISOC) have emerged as suitable platform in this regard [1–15]. The ISOC makes these superconductors robust against in-plane magnetic fields [16–18] much higher than the Pauli limit [19,20]. Therefore, superconductivity in the presence of strong ferromagnetism can be studied in such Ising superconductors. The in-plane field in these materials induces spin-triplet correlations [15,21–25], leading to the prediction of spectral features such as mirage gaps [25–27]. Ferromagnetic (FM) Josephson junctions have been predicted to show 0 and π states, useful to construct ϕ_0 junctions [13,14]. FM Ising superconductor junctions [28,29] and Josephson junctions with half-metal barriers [30,31] focus on spin-triplet Andreev reflection. The charge and spin currents in Ising superconductor Josephson junctions are shown to be field tunable [32].

Andreev bound states (ABSs) exist in the proximity of superconductors, often localized within the region of superconducting barriers, enabling the flow of supercurrent [33,34]. The ABSs play a crucial role in superconducting hybrid structures, opening the possibilities for topologically protected qubits for quantum computation [35–37]. However, the study of ABSs in the Ising superconductor Josephson junctions has received limited attention.

Moreover, recent advancements in the field of diode effect for superconductors have gathered significant attention, in the pursuit of nonreciprocal current transport [38–53]. The breaking of inversion or time-reversal symmetry is necessary for an asymmetric current-phase relation (CPR) as a function of the Josephson phase [46]. A supercurrent interferometer with two junctions with one nonsinusoidal CPR and one sinusodial CPR is the most basic textbook example for a diode effect [42,43]. Note that this proposal requires to flux bias the superconducting quantum interference device (SQUID) for the diode effect to appear.

Motivated by these developments, we explore the ABS spectrum in a single-channel Ising superconductor Josephson junction with a transparent nonmagnetic constriction as shown in Fig. 1(a). The FM layers provide in-plane exchange fields to the superconductors. We obtain the spectrum of ABSs as a function of the Josephson phase in Fig. 1(b). The relative orientation of the in-plane exchange fields present in the superconductors splits the spin-degenerate ABSs. The degree of spin splitting of the ABSs is maximum for antiparallel alignment of the in-plane fields and increases with the strength of the exchange fields. The ABSs diminish with increasing strength of the in-plane fields due to the pair-breaking effect. The behaviors of the ABSs are directly reflected in the CPR which follows a nonsinusoidal behavior [see the red curve in Fig. 1(d)]. The quantum circuit theory [54] is employed to numerically calculate the supercurrent for the system in Fig. 1(a) for arbitrary transparencies. We then construct a different junction by adding a fully spin-polarized FM barrier between the superconductors as shown in Fig. 1(c). The total CPR is then a sum of the CPRs of the nonmagnetic and FM barriers. This results in a nonreciprocal CPR, or diode effect, as seen from Fig. 1(d). The diode efficiency is highly tunable

*Contact author: gmtang@gscaep.ac.cn
†Contact author: wolfgang.belzig@uni-konstanz.de

Published by the American Physical Society under the terms of the Creative Commons Attribution 4.0 International license. Further distribution of this work must maintain attribution to the author(s) and the published article's title, journal citation, and DOI.

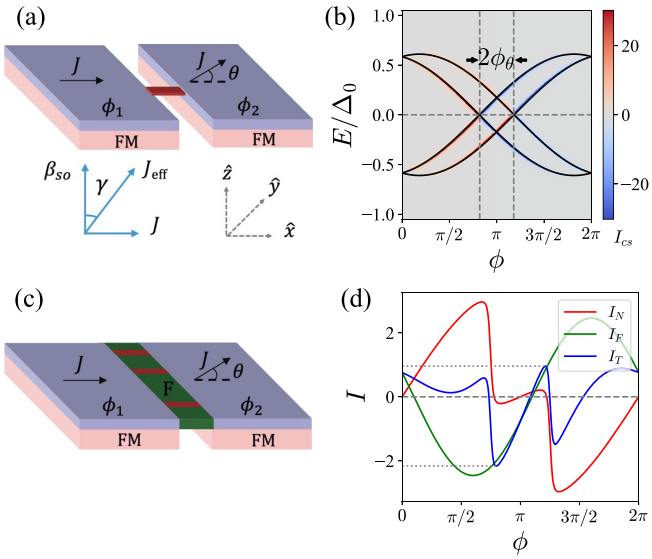


FIG. 1. (a) Schematic plot of the Ising superconductor Josephson junction with a nonmagnetic channel of high transmission. The relative angle between the exchange fields is θ and the phase difference is $\phi = \phi_1 - \phi_2$. The effective exchange field $\boldsymbol{J}_{\text{eff}}$ has an angle γ to spin-orbit coupling. (b) Andreev bound states (black) and spectral supercurrent (color scale) for $\theta = \pi/2$, $\beta_{\text{so}} = 7\Delta_0$, and $J = 3\Delta_0$ (black curve). The spin splitting is parametrized by ϕ_θ illustrating the spin splitting by the noncollinear in-plane exchange fields. (c) Schematic plot of the Andreev-Ising-Josephson junction. A spin-polarized magnetic barrier (in green) and nonmagnetic transmissive channels (in red) connect two superconductors. (d) Current-phase relations for the junctions with a transparent nonmagnetic barrier (red curve) and a ferromagnetic tunneling barrier (green curve). The total current-phase relation (blue) is highly nonreciprocal with positive and negative critical currents I_c indicated by dotted lines. The conductance ratio of the nonmagnetic and the magnetic parts is 1:10, while $J = 3\Delta_0$, $T = 0.01T_c$, and $\theta = 0.9\pi$, and supercurrents are in the units of $2G_0\Delta_0/e$.

by varying the relative orientation of the exchange fields and the conductance ratio between the FM and nonmagnetic barriers. Our system offers a practical approach that eliminates the need for flux piercing, unlike the Josephson diode effects studied earlier in Refs. [42,43].

Andreev bound states. An Ising superconductor in contact with an FM layer, with a singlet order parameter Δ and superconducting phase ϕ_α can be described by a Bogoliubov–de Gennes Hamiltonian near the $\boldsymbol{K}$ ($\boldsymbol{K}'$) valley by neglecting the contribution from the Γ point [15]. The effective Hamiltonian can be written in the Nambu basis $(c_{\boldsymbol{k},\uparrow}, c_{\boldsymbol{k},\downarrow}, c^\dagger_{-\boldsymbol{k},\uparrow}, c^\dagger_{-\boldsymbol{k},\downarrow})$ as

$$H_{\text{BdG}} = \begin{bmatrix} H_0(\boldsymbol{k}) & \Delta e^{i\phi_\alpha} i\sigma_y \\ -\Delta e^{-i\phi_\alpha} i\sigma_y & -H_0^*(-\boldsymbol{k}) \end{bmatrix}, \tag{1}$$

where $H_0(\boldsymbol{k})$ is given by

$$H_0(\boldsymbol{k} = \boldsymbol{p} + s\boldsymbol{K}) = \xi_p \sigma_0 + s\beta_{\text{so}}\sigma_z - \boldsymbol{J}\cdot\boldsymbol{\sigma}. \tag{2}$$

Here, $s = +1$ corresponds to the valley $\boldsymbol{K}$ and $s = -1$ to $\boldsymbol{K}'$. The deviation of the momentum from $\boldsymbol{K}$ or $\boldsymbol{K}'$ is denoted by $\boldsymbol{p}$. The Pauli matrices σ_x, σ_y, and σ_z act on the spin space, and σ_0 is the corresponding unit matrix. The dispersion measured from the chemical potential μ is $\xi_p = |\boldsymbol{p}|^2/2m - \mu$. The ISOC strength is denoted by β_{so}. The Zeeman term $\boldsymbol{J}\cdot\boldsymbol{\sigma}$ arises from the in-plane exchange field $\boldsymbol{J}$ provided by the FM layer. Note that due to the exchange field the main superconducting gap is reduced to $2\Delta_{\text{eff}}$ with $\Delta_{\text{eff}} = \Delta\beta_{\text{so}}/J_{\text{eff}}$ and $J_{\text{eff}} = \sqrt{\beta_{\text{so}}^2 + J^2}$.

We first consider a model based on the scattering approach for two identical Ising superconductors separated by a nonmagnetic scatterer in a single-channel approximation [see Fig. 1(a)]. The two superconductors have identical ISOC and we assume the relative angle between the two exchange fields provided by the two adjacent FM layers is denoted as θ. The condition for ABSs in the junction with ideal transmission can be found through determinant relation [55]

$$\det(1 - R_1 S_1 R_2 S_2) = 0. \tag{3}$$

The Andreev scattering at each superconductor α (=1, 2) is described by a spin rotation matrix R_α and an electron-hole scattering matrix S_α given by

$$R_\alpha = \begin{bmatrix} e^{i\gamma \boldsymbol{n}_\alpha\cdot\boldsymbol{\sigma}} & 0 \\ 0 & e^{-i\gamma \boldsymbol{n}_\alpha\cdot\boldsymbol{\sigma}} \end{bmatrix}, \quad S_\alpha = \begin{bmatrix} 0 & r_e(\phi_\alpha)\sigma_0 \\ r_h(\phi_\alpha)\sigma_0 & 0 \end{bmatrix}. \tag{4}$$

The unit vectors $\boldsymbol{n}_1$ and $\boldsymbol{n}_2$ denote the orientation of the in-plane exchange fields with $\boldsymbol{n}_1 = (1, 0, 0)$ and $\boldsymbol{n}_2 = (\cos\theta, \sin\theta, 0)$. The angle $\gamma = \arccos(\beta_{\text{so}}/J_{\text{eff}})$ is between the z axis and the effective field $\boldsymbol{J}_{\text{eff}}$ as shown in Fig. 1(a). The Andreev reflection coefficients are $r_{e/h}(\phi_\alpha) = \exp(\pm i\phi_\alpha + i\chi)$ with the superconducting phase ϕ_α and $\chi = \arccos(E/\Delta_{\text{eff}})$. Simplifying Eq. (3) we obtain $\phi + 2\chi \pm \phi_\theta = 0$ where $\phi = \phi_1 - \phi_2$ is the Josephson phase and ϕ_θ is the spin-splitting parameter defined as

$$\cos\phi_\theta = \cos^2\gamma + \sin^2\gamma\cos\theta. \tag{5}$$

This leads to the ABS energies given by

$$E = \pm\Delta_{\text{eff}}\cos[(\phi \pm \phi_\theta)/2] \tag{6}$$

and is shown in Fig. 1(b) as a line. The parameter $2\phi_\theta$ denotes the difference between the zero crossing of the ABSs and is due to the interplay between noncollinear exchange fields and ISOC. Obviously, from Eq. (5) the spin-splitting parameter ϕ_θ vanishes at $\theta = 0$ or $J = 0$. Since the function $\arccos(x)$ decreases monotonically in the range of $-1 < x < 1$, ϕ_θ is maximal at $\theta = \pi$ and increases with increasing the exchange fields. The supercurrent carried by spin-split ABSs is given by

$$I_0(\phi) = (2e/\hbar)\sum(\partial E/\partial\phi)\tanh[E/(2k_BT)], \tag{7}$$

where the summation runs over all the four solutions of E in Eq. (6).

To corroborate the simple picture, we perform calculations using quasiclassical Green's functions. In the following, we fix the ISOC strength to $\beta_{\text{so}} = 7\Delta_0$ where Δ_0 is the superconducting gap in the absence of external fields at zero temperature. A broadening parameter of $0.01\Delta_0$ is taken into account. The reduced superconducting order parameter Δ due to the in-plane exchange field and the finite temperature is calculated self-consistently as described in Ref. [32]. The ABSs given by Eq. (6) are shown in Fig. 1(b) for $\theta = \pi/2$ and they overlap the numerically calculated spectral supercurrent obtained using Green's function methods discussed later. The

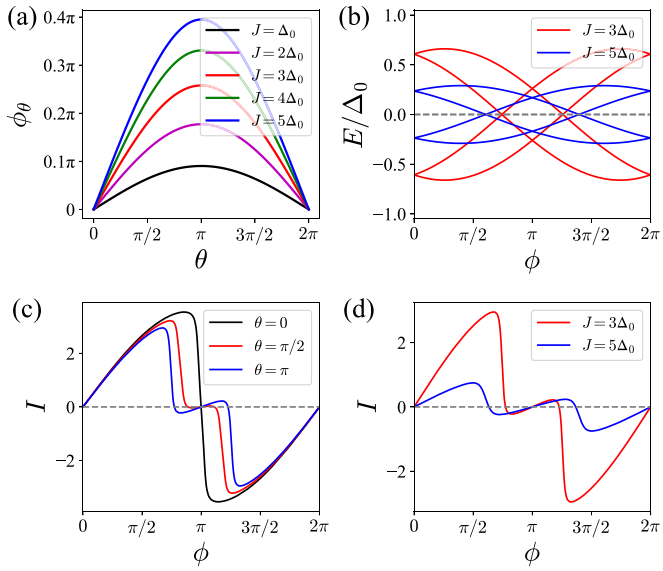


FIG. 2. (a) The spin-splitting parameter ϕ_θ vs the relative magnetization angle θ at different exchange-field strengths J. (b) Andreev bound states at $\theta=\pi$. (c) Current-phase relations for various θ at $J=3\Delta_0$. (d) Current-phase relations at $\theta=\pi$. The supercurrent is in the units of $2G_0\Delta_0/e$. The temperature in (c) and (d) is $T=0.01T_c$.

4π periodic cosine curves in Fig. 1(b) indicate spin-split ABSs with the splitting is characterized by ϕ_θ. Figure 2(a) shows the dependence of ϕ_θ on relative magnetization angle θ for various exchange fields and it agrees with the previous discussion on Eq. (5). The spin splitting is maximal when the in-plane fields are antiparallel, i.e., $\theta=\pi$. Moreover, the splitting increases with the exchange field and reaches a maximum at a critical value where the superconductivity is destroyed. As the superconducting gap diminishes with increasing the exchange fields, the ABSs also diminish as seen from Fig. 2(b). The ABSs eventually vanish at the critical value of the exchange fields.

The analytical treatment above provides results for a perfectly transparent nonmagnetic barrier. We now employ the quantum circuit theory [54,56] to obtain the CPRs at arbitrary transparencies of the junction. The expression of the supercurrent for a single-channel junction with transparency D is given by

$$I(D,\varphi)=\frac{G_0}{8e}\int_{-\infty}^{\infty}d\varepsilon\,\mathrm{tr}[\tau_3\sigma_0\hat{I}^K(\varepsilon)], \tag{8}$$

with $G_0=2e^2/h$ being the conductance quantum. The Keldysh component of the matrix current $\hat{I}^K$ is given by

$$\hat{I}^K=2(\hat{A}^R\hat{X}^K+\hat{A}^K\hat{X}^A), \tag{9}$$

with $\check{A}=2D[\check{g}_2,\check{g}_1]$ and $\check{X}=[4-D(2-\{\check{g}_2,\check{g}_1\})]^{-1}$, where $[\check{g}_2,\check{g}_1]$ is the commutator and $\{\check{g}_2,\check{g}_1\}$ is the anticommutator for the Green's functions. The Green's function $\check{g}_\alpha$ with $\alpha=1,2$ denoting the two superconductors is in Keldysh space and has the structure of

$$\check{g}_\alpha=\begin{pmatrix}\hat{g}_\alpha^R & \hat{g}_\alpha^K\\ 0 & \hat{g}_\alpha^A\end{pmatrix}, \tag{10}$$

where $\hat{g}_\alpha^R$, $\hat{g}_\alpha^A$, and $\hat{g}_\alpha^K$ are, respectively, the retarded, advanced, and Keldysh components of $\check{g}_\alpha(\varepsilon)$. The calculation details for the Green's function are provided in the Supplemental Material [56].

The spectral supercurrent I_{cs} defined as $\mathrm{tr}[\tau_3\sigma_0\hat{I}^K(\varepsilon)]$ for $D=1$ is plotted in Fig. 1(b) and it agrees well with the ABSs given by Eq. (6). To understand how ABSs influence the supercurrent we compute CPRs using Eq. (8) as shown in Fig. 2(c). At the parallel magnetization configuration, we observe the well-known sawtooth shape. The supercurrent becomes increasingly nonsinusoidal as the magnetization configuration changes from parallel to antiparallel as seen in Fig. 2(c). This change directly reflects the increasing spin-splitting of ABSs. For an antiparallel configuration as shown in Fig. 2(c), the current switches parity and vanishes at two different phases other than $\phi=0$ and $\phi=\pi$, due to a pair of ABSs crossing zero energy at these phases. This signifies the presence of the second harmonics in addition to the first one in the CPRs. Figure 2(d) shows the decreasing supercurrent at stronger in-plane fields. This is expected as the diminishing amplitude of the ABSs at higher fields [see Fig. 2(b)] contributes to lower supercurrent.

Superconducting diode effect. A simple approach to obtain nonreciprocal critical currents for forward and reverse biases in a superconducting junction involves utilizing two different CPRs, as discussed in Refs. [42,43]. Specifically, a junction with a CPR that is the sum of two different types: $I\propto\sin(\phi+\phi_0)$ and $I\propto\sin(2\phi)$ with nonvanishing ϕ_0 is required for the diode effect. In our work, we have already achieved CPRs with components of $\sin(2\phi)$ using a transparent nonmagnetic barrier. Previous research [32] has demonstrated that phase-shifted sinusoidal CPR can be realized in an FM-Ising Josephson junction even in the tunneling limit. Based on these findings, below we perform a numerical assessment to achieve the diode effect.

As depicted in Fig. 1(c), we combine a nonmagnetic junction having perfect transmission with an FM junction in the tunneling limit to form a Josephson diode. The nonmagnetic barrier contains N_c transparent channels with conductance $G_N=N_cG_0$ so that the supercurrent is $I_N(\phi)=N_cI(1,\phi)$ obtained from Eq. (8). The FM channels are assumed to be fully spin polarized with a magnetization pointing out of plane. The supercurrent through the FM barrier is expressed as [32,56]

$$I_F=I_{Fc}\sin(\phi+\theta), \tag{11}$$

where I_{Fc} is

$$I_{Fc}=\frac{G_F}{8e}\int_{-\infty}^{\infty}d\varepsilon\,\mathrm{tr}(\tau_3\sigma_0\hat{I}^R)\tanh[\varepsilon/(2k_BT)], \tag{12}$$

with the conductance of the FM tunnel barrier G_F. The retarded matrix current $\hat{I}^R$ is given by

$$\hat{I}^R=\mathrm{Re}\big[\hat{g}_2^R+\{\hat{\kappa},\hat{g}_2^R\}+\hat{\kappa}\hat{g}_2^R\hat{\kappa},\hat{g}_1^R\big], \tag{13}$$

with the spin matrix $\hat{\kappa}=\mathrm{diag}(\sigma_z,\sigma_z)$. The total current I_T in this system would then be

$$I_T=I_N+I_F. \tag{14}$$

It should be noted that the conductances G_N and G_F differ in the number of transmission channels and the transmission

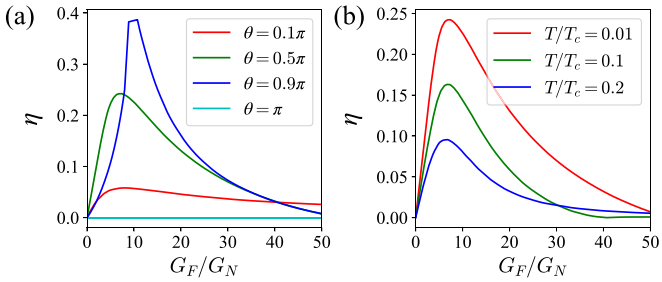


FIG. 3. (a) Efficiency η vs conductance ratio G_F/G_N for different θ at $T = 0.01T_c$. (b) Efficiency η vs G_F/G_N for different temperature T at $\theta = \pi/2$.

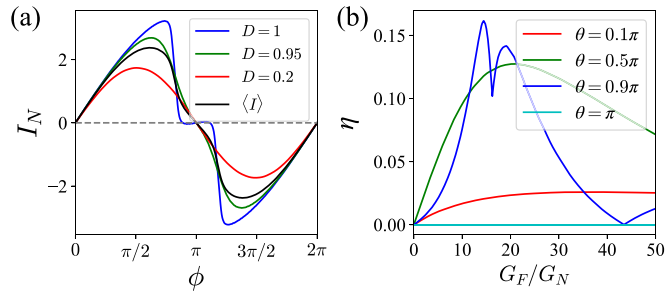


FIG. 4. (a) Current-phase relations for different transparencies of the nonmagnetic barrier with $\theta = \pi/2$. The black curve represents the average current-phase relation using the Dorokhov distribution for a diffusive short junction. The supercurrents are in the units of $2G_N\Delta_0/e$. (b) Efficiency η vs conductance ratio G_F/G_N for different θ where the transmission in the nonmagnetic barrier follows the Dorokhov distribution. The temperature is $T = 0.01T_c$.

values. This implies that the conductance ratio G_F/G_N in principle be controlled by the respective numbers of channels.

The CPRs for I_N, I_F, and I_T are plotted in Fig. 1(d). The CPR for the nonmagnetic barrier with perfect transmission deviates from the sinusoidal behavior. The current vanishes at four values of ϕ including $\phi = 0$ and $\phi = \pi$. The CPR for the FM tunnel barrier is perfectly sinusoidal shifted by the relative magnetization angle θ of the two superconductors. For the total current of the system I_T, there exists a nonreciprocal critical current for forward and reverse bias directions. Thus, a Josephson diode effect can be achieved. The diode efficiency η that measures the nonreciprocity of the critical currents is defined as

$$\eta = \frac{|I_T^+ - I_T^-|}{I_T^+ + I_T^-}, \tag{15}$$

where I_T^+ and I_T^- are, respectively, the absolute values of the maximum and minimum of the total supercurrent I_T. For the case with conductance ratio $G_F/G_N = 10$ and relative exchange-field angle $\theta = 0.9\pi$, the diode efficiency is as large as about 0.4 in Fig. 1(d). In the following, we provide a systematic investigation on the diode efficiency.

Figures 3(a) and 3(b) display the diode efficiency as a function of the conductance ratio for various relative exchange-field angles and temperatures, respectively. The diode efficiency vanishes under the parallel and antiparallel configurations of the exchange fields where the CPR for the FM barrier follows $I_{Fc}\sin\phi$ or $-I_{Fc}\sin\phi$ as shown in Eq. (11). For a given conductance ratio, there is an optimal θ for the largest diode efficiency. The diode efficiency is sensitive to temperature and decreases with it as seen from Fig. 3(b). This is due to the fact that increasing temperature reduces the nonsinusoidal behavior or the second harmonics in the CPR of the nonmagnetic barrier. As shown in Fig. 4(a), the CPR becomes more sinusoidal with decreasing transmission D for the junction of nonmagnetic barrier.

In order to model a more realistic situation we now assume a large number of channels with a distribution of transmissions [57]. As a generic example, we use the Dorokhov distribution of transmissions given by $\rho(D) = G_N/(\pi G_0 D\sqrt{1-D})$ with G_N being the conductance of the diffusive part. The supercurrent for such a short diffusive nonmagnetic barrier is [57]

$$I_N(\phi) = \int_0^1 dD\rho(D)I(D,\phi). \tag{16}$$

The corresponding CPR is displayed as the black curve in Fig. 4(a). Remarkably, the diffusive CPR is still quite nonsinusoidal, which means that the diode efficiency could be substantial. We explore the nonreciprocity of the junction by combining the short diffusive nonmagnetic barrier and an FM tunneling barrier, where the total current is $I_T = I_N + I_F$. As shown in Fig. 4(b), a significant diode efficiency is present in this more realistic disordered many-channel situation [41,47]. This gives hope that our predicted diode effect is robust against disorder and might be accessible to experiments.

Conclusion. We have investigated the transport properties of Ising superconductor Josephson junctions under the influence of in-plane exchange fields. For a Josephson junction with a transparent nonmagnetic constriction, the ABSs are spin split due to the interplay of the exchange fields and ISOCs. The spin splitting can be controlled by the strengths and the relative orientation of the exchange fields. The properties of the ABS are directly reflected in the supercurrent. We further demonstrate a Josephson diode effect by adding an FM tunneling barrier to the Ising superconductor Josephson junction with the nonmagnetic channel of high transmission. The diode efficiency is tunable by varying either the relative exchange-field orientation or the conductance ratio of the barriers. Furthermore, the effect is insensitive to disorder and should be observable in generic Andreev-Ising-Josephson contacts with magnetic elements. Our work provides a practical scheme in realizing the superconducting diode with two-dimensional heterostructures.

Acknowledgments. We acknowledge useful discussions with Michael Hein. S.P. and W.B. acknowledge funding by the Deutsche Forschungsgemeinschaft (DFG, German Research Foundation)–Project-ID 443404566 - SPP 2244. G.T. is supported by National Natural Science Foundation of China (Grants No. 12088101 and No. 12374048) and NSAF (Grant No. U2330401).

[1] J. M. Lu, O. Zheliuk, I. Leermakers, N. F. Q. Yuan, U. Zeitler, K. T. Law, and J. T. Ye, Evidence for two-dimensional Ising superconductivity in gated MoS_2, Science **350**, 1353 (2015).

[2] Y. Saito, Y. Nakamura, M. S. Bahramy, Y. Kohama, J. Ye, Y. Kasahara, Y. Nakagawa, M. Onga, M. Tokunaga, T. Nojima, Y. Yanase, and Y. Iwasa, Superconductivity protected by spin-valley locking in ion-gated MoS_2, Nat. Phys. **12**, 144 (2016).

[3] X. Xi, Z. Wang, W. Zhao, J.-H. Park, K. T. Law, H. Berger, L. Forró, J. Shan, and K. F. Mak, Ising pairing in superconducting $NbSe_2$ atomic layers, Nat. Phys. **12**, 139 (2016).

[4] Y. Xing, K. Zhao, P. Shan, F. Zheng, Y. Zhang, H. Fu, Y. Liu, M. Tian, C. Xi, H. Liu, J. Feng, X. Lin, S. Ji, X. Chen, Q.-K. Xue, and J. Wang, Ising superconductivity and quantum phase transition in macro-size monolayer $NbSe_2$, Nano Lett. **17**, 6802 (2017).

[5] T. Dvir, F. Massee, L. Attias, M. Khodas, M. Aprili, C. H. L. Quay, and H. Steinberg, Spectroscopy of bulk and few-layer superconducting $NbSe_2$ with van der Waals tunnel junctions, Nat. Commun. **9**, 598 (2018).

[6] D. Costanzo, H. Zhang, B. A. Reddy, H. Berger, and A. F. Morpurgo, Tunnelling spectroscopy of gate-induced superconductivity in MoS_2, Nat. Nanotechnol. **13**, 483 (2018).

[7] J. Lu, O. Zheliuk, Q. Chen, I. Leermakers, N. E. Hussey, U. Zeitler, and J. Ye, Full superconducting dome of strong Ising protection in gated monolayer WS_2, Proc. Natl. Acad. Sci. USA **115**, 3551 (2018).

[8] S. C. de la Barrera, M. R. Sinko, D. P. Gopalan, N. Sivadas, K. L. Seyler, K. Watanabe, T. Taniguchi, A. W. Tsen, X. Xu, D. Xiao, and B. M. Hunt, Tuning Ising superconductivity with layer and spin-orbit coupling in two-dimensional transition-metal dichalcogenides, Nat. Commun. **9**, 1427 (2018).

[9] E. Sohn, X. Xi, W.-Y. He, S. Jiang, Z. Wang, K. Kang, J.-H. Park, H. Berger, L. Forró, K. T. Law, J. Shan, and K. F. Mak, An unusual continuous paramagnetic-limited superconducting phase transition in 2D $NbSe_2$, Nat. Mater. **17**, 504 (2018).

[10] J. Li, H.-B. Leng, H. Fu, K. Watanabe, T. Taniguchi, X. Liu, C.-X. Liu, and J. Zhu, Superconducting proximity effect in a transparent van der Waals superconductor-metal junction, Phys. Rev. B **101**, 195405 (2020).

[11] C.-W. Cho, J. Lyu, L. An, T. Han, K. T. Lo, C. Y. Ng, J. Hu, Y. Gao, G. Li, M. Huang, N. Wang, J. Schmalian, and R. Lortz, Nodal and nematic superconducting phases in $NbSe_2$ monolayers from competing superconducting channels, Phys. Rev. Lett. **129**, 087002 (2022).

[12] A. Hamill, B. Heischmidt, E. Sohn, D. Shaffer, K.-T. Tsai, X. Zhang, X. Xi, A. Suslov, H. Berger, L. Forró, F. J. Burnell, J. Shan, K. F. Mak, R. M. Fernandes, K. Wang, and V. S. Pribiag, Two-fold symmetric superconductivity in few-layer $NbSe_2$, Nat. Phys. **17**, 949 (2021).

[13] H. Idzuchi, F. Pientka, K.-F. Huang, K. Harada, O. Gül, Y. J. Shin, L. T. Nguyen, N. H. Jo, D. Shindo, R. J. Cava, P. C. Canfield, and P. Kim, Unconventional supercurrent phase in Ising superconductor Josephson junction with atomically thin magnetic insulator, Nat. Commun. **12**, 5332 (2021).

[14] L. Ai, E. Zhang, C. Huang, X. Xie, Y. Yang, Z. Jia, Y. Zhang, S. Liu, Z. Li, P. Leng, X. Sun, X. Kou, Z. Han, and F. Xiu, Van der Waals ferromagnetic Josephson junctions, Nat. Commun. **12**, 6580 (2021).

[15] M. Kuzmanović, T. Dvir, D. LeBoeuf, S. Ilić, M. Haim, D. Möckli, S. Kramer, M. Khodas, M. Houzet, J. S. Meyer, M. Aprili, H. Steinberg, and C. H. L. Quay, Tunneling spectroscopy of few-monolayer $NbSe_2$ in high magnetic fields: Triplet superconductivity and Ising protection, Phys. Rev. B **106**, 184514 (2022).

[16] L. N. Bulaevskii, A. A. Guseinov, and A. I. Rusinov, Superconductivity in crystals without symmetry centers, Sov. Phys. JETP **44**, 1243 (1976) [Zh. Eksp. Teor. Fiz. **71**, 2356 (1976)].

[17] L. P. Gor'kov and E. I. Rashba, Superconducting 2D system with lifted spin degeneracy: Mixed singlet-triplet state, Phys. Rev. Lett. **87**, 037004 (2001).

[18] P. A. Frigeri, D. F. Agterberg, A. Koga, and M. Sigrist, Superconductivity without inversion symmetry: MnSi versus $CePt_3Si$, Phys. Rev. Lett. **92**, 097001 (2004).

[19] B. S. Chandrasekhar, A note on the maximum critical field of high-field superconductors, Appl. Phys. Lett. **1**, 7 (1962).

[20] A. M. Clogston, Upper limit for the critical field in hard superconductors, Phys. Rev. Lett. **9**, 266 (1962).

[21] M. A. Rahimi, A. G. Moghaddam, C. Dykstra, M. Governale, and U. Zülicke, Unconventional superconductivity from magnetism in transition-metal dichalcogenides, Phys. Rev. B **95**, 104515 (2017).

[22] D. Möckli and M. Khodas, Robust parity-mixed superconductivity in disordered monolayer transition metal dichalcogenides, Phys. Rev. B **98**, 144518 (2018).

[23] D. Möckli and M. Khodas, Ising superconductors: Interplay of magnetic field, triplet channels, and disorder, Phys. Rev. B **101**, 014510 (2020).

[24] M. Haim, D. Möckli, and M. Khodas, Signatures of triplet correlations in density of states of Ising superconductors, Phys. Rev. B **102**, 214513 (2020).

[25] G. Tang, C. Bruder, and W. Belzig, Magnetic field-induced "mirage" gap in an Ising superconductor, Phys. Rev. Lett. **126**, 237001 (2021).

[26] S. Patil, G. Tang, and W. Belzig, Spectral properties of a mixed singlet-triplet Ising superconductor, Front. Electron. Mater. **3**, 1254302 (2023).

[27] S. Ilić, J. S. Meyer, and M. Houzet, Spectral properties of disordered Ising superconductors with singlet and triplet pairing in in-plane magnetic fields, Phys. Rev. B **108**, 214510 (2023).

[28] B. T. Zhou, N. F. Q. Yuan, H.-L. Jiang, and K. T. Law, Ising superconductivity and Majorana fermions in transition-metal dichalcogenides, Phys. Rev. B **93**, 180501(R) (2016).

[29] P. Lv, Y.-F. Zhou, N.-X. Yang, and Q.-F. Sun, Magnetoanisotropic spin-triplet Andreev reflection in ferromagnet-Ising superconductor junctions, Phys. Rev. B **97**, 144501 (2018).

[30] Q. Cheng and Q.-F. Sun, Switch effect and 0-π transition in Ising superconductor Josephson junctions, Phys. Rev. B **99**, 184507 (2019).

[31] S. Acharjee, A. Boruah, N. Dutta, and R. Devi, Tunability of Andreev levels in a spin-active Ising superconductor/half-metal Josephson junction, Supercond. Sci. Technol. **36**, 125014 (2023).

[32] G. Tang, R. L. Klees, C. Bruder, and W. Belzig, Controlling charge and spin transport in an Ising-superconductor Josephson junction, Phys. Rev. B **104**, L241413 (2021).

[33] C. W. J. Beenakker and H. van Houten, Josephson current through a superconducting quantum point contact shorter than the coherence length, Phys. Rev. Lett. **66**, 3056 (1991).

[34] A. Furusaki and M. Tsukada, Current-carrying states in Josephson junctions, Phys. Rev. B **43**, 10164 (1991).
[35] N. M. Chtchelkatchev and Y. V. Nazarov, Andreev quantum dots for spin manipulation, Phys. Rev. Lett. **90**, 226806 (2003).
[36] A. Zazunov, V. S. Shumeiko, E. N. Bratus', J. Lantz, and G. Wendin, Andreev level qubit, Phys. Rev. Lett. **90**, 087003 (2003).
[37] C. Padurariu and Y. V. Nazarov, Theoretical proposal for superconducting spin qubits, Phys. Rev. B **81**, 144519 (2010).
[38] R. Grein, M. Eschrig, G. Metalidis, and G. Schön, Spin-dependent Cooper pair phase and pure spin supercurrents in strongly polarized ferromagnets, Phys. Rev. Lett. **102**, 227005 (2009).
[39] T. Yokoyama, M. Eto, and Y. V. Nazarov, Anomalous Josephson effect induced by spin-orbit interaction and Zeeman effect in semiconductor nanowires, Phys. Rev. B **89**, 195407 (2014).
[40] F. Dolcini, M. Houzet, and J. S. Meyer, Topological Josephson ϕ_0 junctions, Phys. Rev. B **92**, 035428 (2015).
[41] F. Ando, Y. Miyasaka, T. Li, J. Ishizuka, T. Arakawa, Y. Shiota, T. Moriyama, Y. Yanase, and T. Ono, Observation of superconducting diode effect, Nature (London) **584**, 373 (2020).
[42] Y. V. Fominov and D. S. Mikhailov, Asymmetric higher-harmonic SQUID as a Josephson diode, Phys. Rev. B **106**, 134514 (2022).
[43] R. S. Souto, M. Leijnse, and C. Schrade, Josephson diode effect in supercurrent interferometers, Phys. Rev. Lett. **129**, 267702 (2022).
[44] A. Daido, Y. Ikeda, and Y. Yanase, Intrinsic superconducting diode effect, Phys. Rev. Lett. **128**, 037001 (2022).
[45] S. Ilić and F. S. Bergeret, Theory of the supercurrent diode effect in Rashba superconductors with arbitrary disorder, Phys. Rev. Lett. **128**, 177001 (2022).
[46] Y. Zhang, Y. Gu, P. Li, J. Hu, and K. Jiang, General theory of Josephson diodes, Phys. Rev. X **12**, 041013 (2022).
[47] H. Wu, Y. Wang, Y. Xu, P. K. Sivakumar, C. Pasco, U. Filippozzi, S. S. P. Parkin, Y.-J. Zeng, T. McQueen, and M. N. Ali, The field-free Josephson diode in a van der Waals heterostructure, Nature (London) **604**, 653 (2022).
[48] E. Strambini, M. Spies, N. Ligato, S. Ilić, M. Rouco, C. González-Orellana, M. Ilyn, C. Rogero, F. S. Bergeret, J. S. Moodera, P. Virtanen, T. T. Heikkilä, and F. Giazotto, Superconducting spintronic tunnel diode, Nat. Commun. **13**, 2431 (2022).
[49] C. Baumgartner, L. Fuchs, A. Costa, S. Reinhardt, S. Gronin, G. C. Gardner, T. Lindemann, M. J. Manfra, P. E. F. Junior, D. Kochan, J. Fabian, N. Paradiso, and C. Strunk, Supercurrent rectification and magnetochiral effects in symmetric Josephson junctions, Nat. Nanotechnol. **17**, 39 (2022).
[50] J. J. He, Y. Tanaka, and N. Nagaosa, A phenomenological theory of superconductor diodes, New J. Phys. **24**, 053014 (2022).
[51] N. F. Q. Yuan and L. Fu, Supercurrent diode effect and finite-momentum superconductors, Proc. Natl. Acad. Sci. USA **119**, e2119548119 (2022).
[52] M. Davydova, S. Prembabu, and L. Fu, Universal Josephson diode effect, Sci. Adv. **8**, eabo0309 (2022).
[53] M. Coraiola, A. E. Svetogorov, D. Z. Haxell, D. Sabonis, M. Hinderling, S. C. ten Kate, E. Cheah, F. Krizek, R. Schott, W. Wegscheider, J. C. Cuevas, W. Belzig, and F. Nichele, Flux-tunable Josephson diode effect in a hybrid four-terminal Josephson junction, ACS Nano **18**, 9221 (2024).
[54] Y. V. Nazarov, Novel circuit theory of Andreev reflection, Superlattices Microstruct. **25**, 1221 (1999).
[55] C. W. J. Beenakker, Universal limit of critical-current fluctuations in mesoscopic Josephson junctions, Phys. Rev. Lett. **67**, 3836 (1991).
[56] See Supplemental Material at http://link.aps.org/supplemental/10.1103/PhysRevB.111.L060502 for the details of the quasiclassical Green's function, and which includes Refs. [58–62].
[57] Y. V. Nazarov and Y. Blanter, *Quantum Transport: Introduction to Nanoscience* (Cambridge University Press, Cambridge, UK, 2009).
[58] G. Eilenberger, Transformation of Gorkov's equation for type II superconductors into transport-like equations, Z. Phys. **214**, 195 (1968).
[59] A. I. Larkin and Y. N. Ovchinnikov, Quasiclassical method in the theory of superconductivity, JETP **28**, 1200 (1969) [Zh. Eksp. Teor. Fiz. **55**, 2262 (1968)].
[60] W. Belzig, F. K. Wilhelm, C. Bruder, G. Schön, and A. D. Zaikin, Quasiclassical Green's function approach to mesoscopic superconductivity, Superlattices Microstruct. **25**, 1251 (1999).
[61] N. Kopnin, *Theory of Nonequilibrium Superconductivity* (Oxford University Press, Oxford, UK, 2001).
[62] M. Eschrig, Spin-polarized supercurrents for spintronics: a review of current progress, Rep. Prog. Phys. **78**, 104501 (2015).